Title:

Determining causal genes from GWAS signals using topologically associating domains

Authors:

Gregory P. Way[1,2], Daniel W. Youngstrom[3], Kurt D. Hankenson[3], Casey S. Greene[2]*, and Struan F.A. Grant[4,5]*

* These authors directed this work jointly

Affiliations:

[1]Genomics and Computational Biology Graduate Program, University of Pennsylvania, Philadelphia, PA 19104, USA

[2]Department of Systems Pharmacology and Translational Therapeutics, University of Pennsylvania, Philadelphia, PA 19104, USA

[3]Department of Small Animal Clinical Sciences, College of Veterinary Medicine, Michigan State University, East Lansing, MI 48824, USA

[4]Department of Pediatrics, Perelman School of Medicine, University of Pennsylvania, Philadelphia, PA 19104, USA

[5]Division of Human Genetics, Division of Endocrinology and Diabetes, The Children's Hospital of Philadelphia, Philadelphia, PA 19104, USA

Author Emails:

GPW: gregway@mail.med.upenn.edu; DWY: dwy@msu.edu; KDH: kdhank@msu.edu; CSG: csgreene@mail.med.upenn.edu; *SFAG: grants@email.chop.edu

Co-Corresponding Authors:*

Struan F.A. Grant

Rm 1102D, 3615 Civic Center Blvd
Philadelphia, PA 19104
Office: 267-426-2795
Fax: 215-590-1258

Casey S. Greene

10-131 SCTR 34th and Civic Center Blvd,
Philadelphia, PA 19104
Office: 215-573-2991
Fax: 215-573-9135

Abstract:

Background

Genome wide association studies (GWAS) have contributed significantly to the field of complex disease genetics. However, GWAS only report signals associated with a given trait and do not necessarily identify the precise location of culprit genes. As most association signals occur in non-coding regions of the genome, it is often challenging to assign genomic variants to the underlying causal mechanism(s). Topologically associating domains (TADs) are primarily cell-type independent genomic regions that define interactome boundaries and can aid in the designation of limits within which a GWAS locus most likely impacts gene function.

Results

We describe and validate a computational method that uses the genic content of TADs to assign GWAS signals to likely causal genes. Our method, called "TAD_Pathways", performs a Gene Ontology (GO) analysis over all genes that reside within the boundaries of all TADs corresponding to the GWAS signals for a given trait or disease. We applied our pipeline to the GWAS catalog entries associated with bone mineral density (BMD), identifying 'Skeletal System Development' (Benjamini-Hochberg adjusted $p = 1.02 \times 10^{-5}$) as the top ranked pathway. Often, the causal gene identified at a given locus was well known and/or the nearest gene to the sentinel SNP. In other cases, our method implicated a gene further away. Our molecular

experiments describe a novel example: *ACP2*, implicated at the canonical '*ARHGAP1*' locus. We found *ACP2* to be an important regulator of osteoblast metabolism, whereas a causal role of *ARHGAP1* was not supported.

Conclusions

Our results demonstrate how basic principles of three-dimensional genome organization can help define biologically informed windows of signal association. We anticipate that incorporating TADs will aid in refining and improving the performance of a variety of algorithms that linearly interpret genomic content.

Keywords:

Genome wide association study, gene prioritization, topologically associating domains, pathway analysis, bone mineral density

Background:

Genome-wide association studies (GWAS) have been applied to over 300 different traits, leading to the discovery and subsequent validation of several important disease associations [1]. However, GWAS can only discover association signals in the data. Subsequent assignment of signal to causal genes has proven difficult due to these signals falling principally within noncoding genomic regions [2–4] and not necessarily implicating the nearest gene [5]. For example, a signal found within an intron for *FTO*, a well-studied gene previously thought to be important for obesity [6], has been shown to physically interact with and lead to the differential expression of two genes (*IRX3* and *IRX5*) directly next to this gene, and not *FTO* itself [7–9]. Moreover, there is evidence suggesting a type 2 diabetes GWAS association previously implicating *TCF7L2* [10] also influences the nearby *ACSL5* gene [11]. It remains unclear how

pervasive these kinds of associations are, but similar strategies are necessary in order for GWAS to better guide research and precision medicine [12].

Three-dimensional genomics has changed the way geneticists think about genome organization and its functional implications [13,14]. Genome-wide chromatin interaction maps have facilitated the development of several genome organization principles, including topologically associating domains (TADs) [15–18]. TADs are sub-architectural units of the overall genome organization that have consistent and functionally important genomic element distributions including an enrichment of housekeeping genes, insulator elements, and early replication timing regions at boundary regions [19–21]. TADs are largely consistent across different cell types and demonstrate synteny [22,23]. These observations can therefore allow the leveraging of TADs to set the bounds of where non-coding causal variants can most likely impact promoters, enhancers and genes in a tissue independent fashion [24,25]. Therefore, we sought to develop a method that integrates GWAS data with interactome boundaries to more accurately map signals to the mostly likely candidate gene(s).

We developed a computational approach, called "TAD_Pathways", which is agnostic to gene locations relative to each GWAS signal within TADs. We scanned publically available GWAS data for given traits and used TAD boundaries to output lists of genes likely to be causal. We demonstrate this approach by assessing the influence of GWAS signals on bone mineral density (BMD) [26–29]. This trait is clinically of great importance as low BMD is an important precursor to osteoporosis, a disease condition affecting millions of patients annually [30]. We also chose BMD as a trait for analysis because BMD GWAS primarily points to very well-known genes involved in bone development (positive controls) but there remain a number of established loci where no obvious gene resides, therefore offering the opportunity to uncover

novel biology. After applying our TAD_Pathways discovery approach, we investigated putative causal genes using cell culture-based assays, identifying *ACP2* as a novel regulator of osteoblast metabolism.

Results:

The Genomic Landscape of SNPs across Topologically Associating Domains

We observed a consistent and non-random distribution of SNPs across TADs derived from human embryonic stem cells (hESC), human fibroblasts (IMR90), mouse embryonic stem cells (mESC), and mouse cortex cells (mcortex) cells. As expected, SNPs are tightly associated with TAD length for each cell type, but there are substantial outlier TADs (**Figure 1**). For example, the TAD harboring the largest number of common SNPs (minor allele frequency (MAF) greater than 0.05) in hESC is located on chromosome 6 (UCSC hg19: chr6:31492021-32932022) and has 19,431 SNPs. Not surprisingly, this TAD harbors an abundance of genes including *HLA* genes, which are well known to have many polymorphic sites [31]. However, the other human cell line (IMR90) outlier TAD is located on chromosome 8 (UCSC hg19: chr8:2132593-6252592) and has 27,220 SNPs and could be potentially biologically meaningful. Indeed, although this TAD harbors relatively few genes, it does include *CSMD1*, a gene implicated in cancer and neurological disorders such as epilepsy and schizophrenia [32,33].

Common SNPs were enriched near the center of TADs (**Figure 1A**). This is the opposite of gene (**Supplementary Figure S1**) and repeat element (**Supplementary Figure S2**) distributions (also see Dixon *et al.* 2012) [22]. The repeat element distribution was driven largely by the SINE/Alu repeat distribution, which could not be explained by GC content and estimated evolutionary divergence (**Supplementary Figure S3**). We also observed that common SNPs are

significantly enriched in the 3' half of TADs in hESC and mcortex cells (**Supplementary Table S1**). There was also a slight increase in GWAS implicated SNPs near hESC TAD boundaries (**Figure 1B**). Given the non-random patterns observed across the TADs, we went on to explore the gene content further in an attempt to imply causality at given GWAS loci.

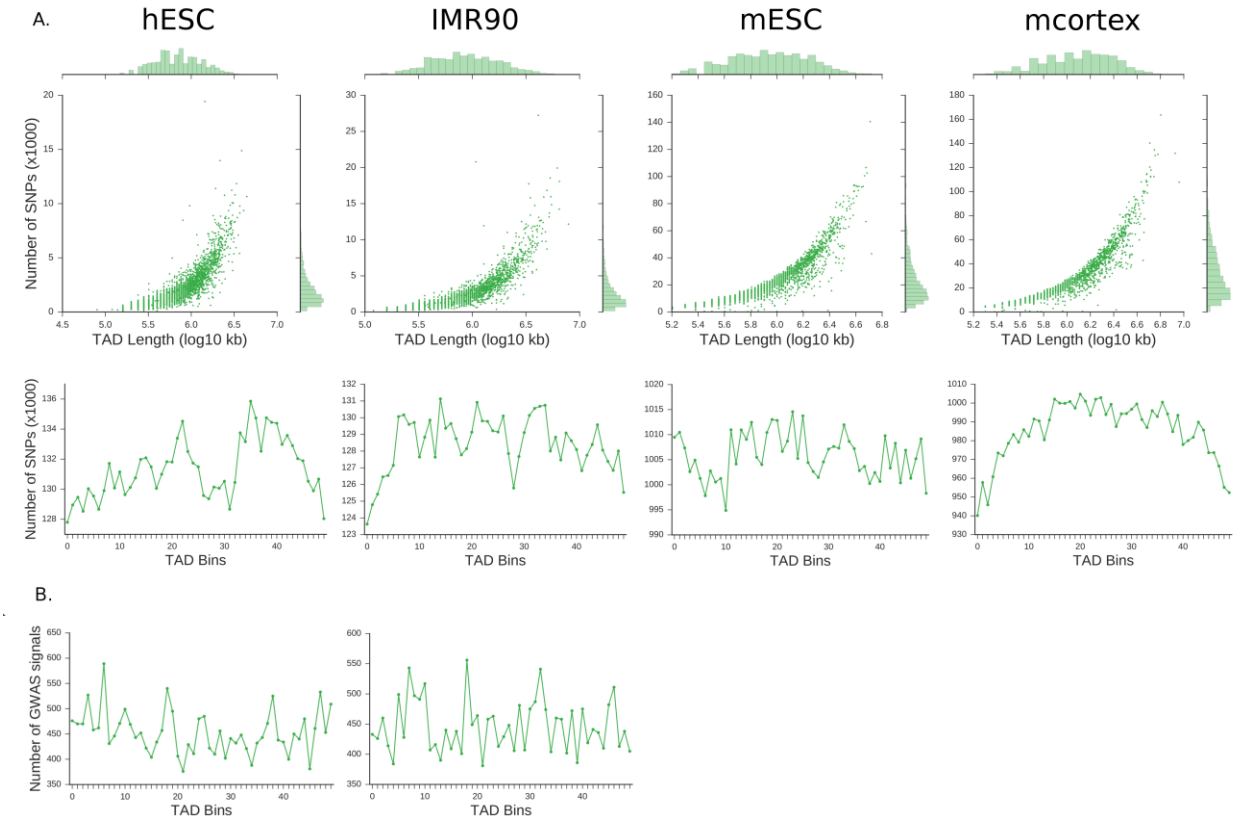

Figure 1. *Distributions of single nucleotide polymorphisms (SNPs) across topologically associating domains of four cell types.* **(A)** Top **–** The length of TADs is associated with the number of SNPs found in each cell type. Bars on the top and right side of the plots represent histograms of each respective metric. hESC and IMR90 TADs are based on 1000 genomes phase 3 SNPs (hg19) and mESC and mcortex TADs represent 15 strains from the mouse genomes project version 2 (mm9). Bottom – Number of SNPs found in each cell type. **(B)** Number of GWAS SNPs from the NHGRI-EBI GWAS catalog that reached genome-wide significance in replication required journals. In each case, we independently discretized TADs into 50 bins where the distribution of elements is linear from 5' to 3' (bin 0 is the 5' most end of all TADs).

TAD_Pathways reveals potentially causal genes within phenotype-associated TADs

Seeking to leverage TADs and disease associated SNPs, we integrated GWAS and TAD domain boundaries in an effort to assign GWAS signals to causal genes. Alternative approaches to understand the gene landscape of a locus that do not consider TAD boundaries typically either assign genes to a GWAS signal based on nearest gene [34] or by an arbitrary or a linkage disequilibrium-based window of several kilobases [35,36] (**Figure 2A**). Instead, we used TAD boundaries and the full catalog of GWAS findings for a given trait or disease to assign genes to GWAS variants based on overrepresentation in a gene set in an approach we termed "TAD_Pathways". For a given trait or disease, we collected all genes that are located in TADs harboring significant GWAS signals. We then applied a statistical enrichment analysis for biological pathways using this TAD gene set and assign candidate genes within a TAD based on the pathways significantly associated with a phenotype (**Figure 2B**). In our implementation, we used GO biological processes, GO cellular components, and GO molecular functions to provide the pathway sets [37]. We included both experimentally confirmed and computationally inferred GO gene annotations, which permit the inclusion of putative casual genes that do not necessarily have literature support but are predicted by a variety of computational methods.

To validate our approach, we applied TAD_Pathways to bone mineral density (BMD) GWAS results derived from replication-requiring journals [26–29]. Our method implicated 'Skeletal System Development' (Benjamini-Hochberg adjusted $p = 1.02 \times 10^{-5}$) as the top ranked pathway. We provide full TAD_Pathways results for BMD in **Supplementary Table S2**. Despite a high content of presumably non-causal genes, which we expect would contribute noise to the overrepresentation analysis [38], our method demonstrated enrichment of a skeletal system related pathway and selected a subset of potentially causal genes belonging to the same pathway.

Many of these genes (24/38) were not the nearest gene to the GWAS signal and several also had independent expression quantitative trail loci (eQTL) support (**Supplementary Table S3, Supplementary Figure S4**).

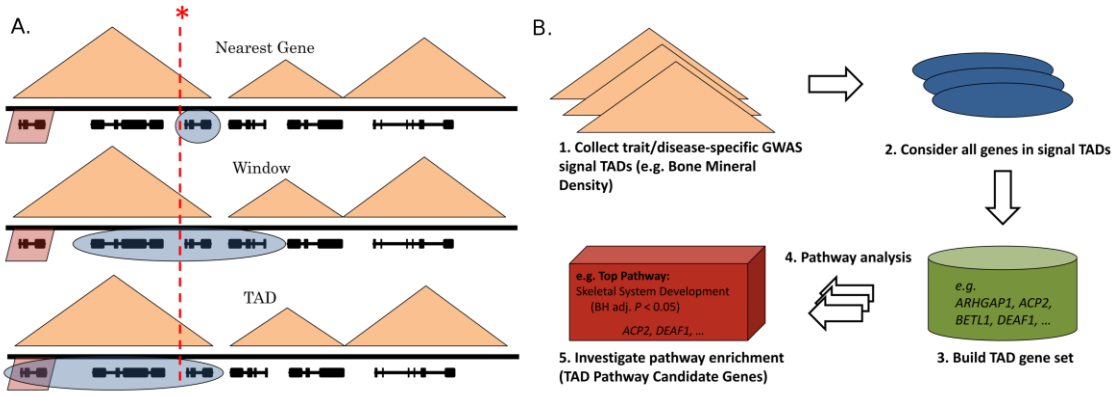

Figure 2. *Concepts motivating our approach.* Topologically associating domains (TADS) are shown as orange triangles, genes are shown as black lines, and a genome wide significant GWAS signal is shown as a dotted red line. **(A)** Three hypothetical examples illustrated by a cartoon. The ground truth causal gene is shaded in red. The method-specific selected genes are shaded in blue. The top panel describes a nearest gene approach. The nearest gene in this scenario is not the gene actually impacted by the GWAS SNP. The middle panel describes a window approach. Based either on linkage disequilibrium or an arbitrarily sized window, the scenario does not capture the true gene. The bottom panel describes the TAD_Pathways approach. In this scenario, the causal gene is selected for downstream assessment. **(B)** The TAD_Pathways method. An example using Bone Mineral Density GWAS signals is shown.

siRNA Knockdown of TAD Pathway Gene Predictions in Osteoblast Cells

The loci rs7932354 (cytoband: 11p11.2) and rs11602954 (cytoband: 11p15.5) are currently assigned to *ARHGAP1* and *BETL1* but our method implicated *ACP2* and *DEAF1*, respectively. The two genes implicated by TAD_Pathways, *ACP2* and *DEAF1*, lacked eQTL support and were not the nearest gene to the BMD GWAS signal. We tested the gene expression activity and metabolic importance of these four genes, *ARHGAP1*, *BETL1*, *DEAF1*, and *ACP2*. Specifically, our assays in a human fetal osteoblast cell line (hFOB) evaluate whether or not the

177 TAD_Pathways method identifies causal genes at GWAS signals beyond those captured by
178 closest and eQTL connected genes. Though these two genes were annotated to the identified GO
179 process, the annotation had been made computationally and their known biology did not provide
180 obvious links to bone biology.

181 We targeted the expression of all four of these genes *in vitro* using small interfering RNA
182 (siRNA), assessing knockdown efficiency at the mRNA level relative to untreated controls and
183 determined corresponding *p* values relative to scrambled siRNA controls. We used an siRNA
184 targeting tissue-nonspecific alkaline phosphatase (*TNAP*) as a positive control. Knockdown
185 efficiencies were: *TNAP* siRNA 48.7±9.9% (p=0.141), *ARHGAP1* siRNA 68.7±14.3%
186 (p=0.015), *ACP2* siRNA 48.9±6.4% (p=0.035), *BET1L* 56.4±1.0% (N.S.) and *DEAF1*
187 52.7±9.2% (p=0.021) (**Figure 3**). siRNA targeted against each gene of interest did not down-
188 regulate the expression of the other genes under investigation, indicating specificity of
189 knockdown, although we noted that *TNAP* siRNA did reduce *DEAF1* gene expression, though
190 this did not reach the threshold for statistical significance (p= 0.077).

191 We noted significant variation across the three controls, with the scrambled siRNA control
192 altering expression of *OCN* (osteocalcin), *IBSP* (bone sialoprotein), *TNAP* and *BET1L* ($p < 0.05$).
193 Relative to the scrambled siRNA control, *OCN* was downregulated in all siRNA groups ($p <$
194 0.05) except for *BET1L* siRNA (p = 0.122). *OSX*, *IBSP* and *TNAP* were not significantly altered
195 by any siRNA treatment (**Figure 3**).
196
197 *Metabolic Activity of TAD Pathway Gene Predictions*
198 Use of *ACP2* siRNA led to a 66.0% reduction in MTT metabolic activity versus the
199 scrambled siRNA control (p = 0.012). *ARHGAP1* siRNA caused a 38.8% reduction, which fell

short of statistical significance ($p = 0.088$). siRNA targeted against *TNAP*, *BET1L* or *DEAF1* did not alter MTT metabolic activity (**Figure 4A**).

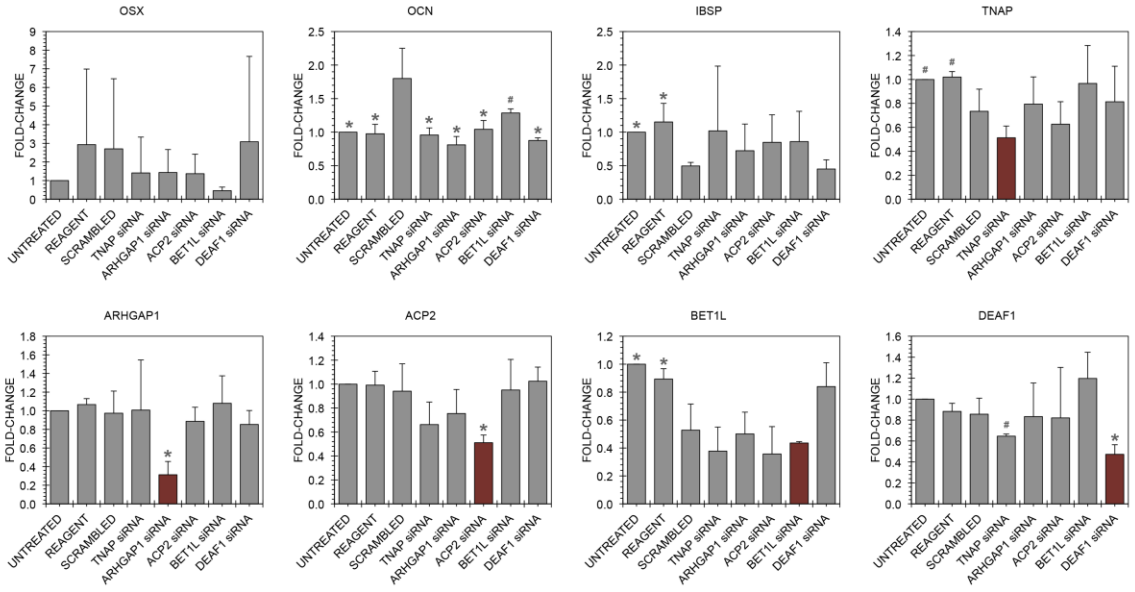

Figure 3: *Real-time PCR of osteoblast differentiation genes and GWAS/TAD hits in hFOB cells.* siRNA was used to knock down expression of *TNAP* (positive control), *ARHGAP1*, *ACP2*, *BET1L* and *DEAF1*. Relative expression of the osteoblast marker genes *OSX*, *OCN* and *IBSP* suggest that GWAS/TAD hits are not major regulators of bone differentiation in this model. Red bars highlight specificity of each siRNA knockdown. Values represent mean ± standard deviation. Statistical significance relative to the scrambled siRNA control is annotated as: *$p \leq 0.05$ and #$p \leq 0.10$ using a two-tailed Student's *t*-test.

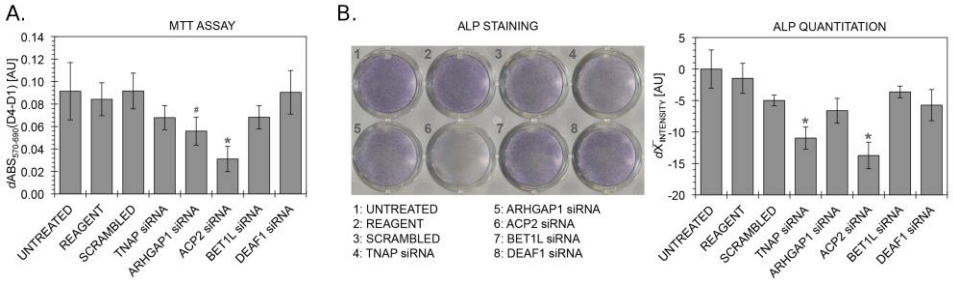

Figure 4. *Validating two 'TAD Pathway' predictions for Bone Mineral Density GWAS hits on hFOB cells.* siRNA was used to knock down expression of *TNAP*, *ARHGAP1*, *ACP2*, *BET1L* and *DEAF1*. **(A)** Knockdown of *ACP2* decreases cellular metabolic activity, demonstrated using an MTT assay. **(B)** ALP staining and quantitation indicates that knockdown of *TNAP* or *ACP2* inhibits performance in an osteoblast differentiation assay. Values represent mean ± standard deviation. Statistical significance relative to the scrambled siRNA control is annotated as: *$p \leq 0.05$ and #$p \leq 0.10$ using a two-tailed Student's *t*-test.

Influence of TAD_Pathways Gene Predictions on Alkaline Phosphatase Activity

Alkaline phosphatase (ALP) is highly expressed in osteoblasts; disruption of proliferation or osteoblast differentiation would result in downregulation of ALP. Treatment with siRNA resulted in changes in ALP staining that we analyzed further by quantitation. *TNAP* siRNA significantly reduced ALP by 5.98±1.77 versus the scrambled siRNA control ($p = 0.006$). *ACP2* siRNA also significantly reduced ALP intensity by 8.74±2.11 versus the scrambled siRNA control ($p = 0.003$). The scrambled siRNA group stained less intensely than untreated or transfection reagent control wells, but this did not reach statistical significance ($0.05 < p < 0.10$) (**Figure 4B**).

Discussion:

We observed a nonrandom enrichment of SNPs in the center of TADs that was consistent across different cell types, but was in the opposite direction of the gene and repeat elements distributions. It is possible that the gene distribution is driving this phenomenon, since coding regions are under higher evolutionary constraint and are thus more averse to SNPs [39]. Nevertheless, GWAS SNPs also appeared to be distributed closely to boundary regions in hESC cells. This may support GWAS causally implicating nearest genes more frequently since genes are also distributed near boundaries. The observation may also suggest that polymorphism in regions near TAD boundaries are more important drivers of disease risk associations than polymorphism in the center of TADs. However, we do not observe this pattern in IMR90 cells. The SNP distribution was also opposite of the SINE/Alu repeat distribution. Given that Alu elements tend to insert into GC-rich regions [40], we tracked GC content across TADs and observed only a slight increase in GC content near TAD boundaries. There was also a slightly

inverse distribution of Alu evolutionary divergence [40]. Our results suggest that the Alu distribution is primarily driven by intronic clustering [41] rather than GC-biased insertion or evolutionary divergence. Recently, retrotransposons have been shown to act as genomic insulators [42], while Alu repeats have been shown to be correlated with functional elements [43]. However, the relationships between polymorphic sites, repeat elements, and genes across TADs and higher level genome organization have yet to be explored in detail and warrants further investigation.

TAD boundaries offer a unique computational opportunity to use biologically informed windows to predefine areas of the genome that are more likely to interact with themselves. We showed, as a proof of concept, that TADs can reveal functional GWAS variant to gene relationships using BMD. Several of the TAD_Pathways implicated genes, including *LRP5* and other Wnt signaling genes, are *bona fide* BMD genes already identified by nearest gene GWAS, eQTL analyses and human clinical syndromes [44,45], thus providing positive controls for our approach. However, several BMD GWAS signals do not have obvious nearest gene associations, which allowed us to validate our approach with two candidate causal, non-nearest gene predictions: *ACP2* and *DEAF1*. Both genes also did not have eQTL associations, but this is likely a result of the eQTL browser lacking bone tissue.

To assess the validity of our predictions, we experimentally knocked down *ACP2* and *DEAF1* in hFOB cells. siRNA for *ACP2* and *DEAF1* did not significantly alter expression of the osteoblast marker genes *OSX, IBSP* or *TNAP*. *OCN* was downregulated in each of the experimental groups relative to the scrambled siRNA control, but comparison with the reagent control indicated no significant difference in any group, suggesting an off-target effect on *OCN* in the scrambled siRNA group. Because osteoblast differentiation genes were not downregulated

following knockdown of the genes of interest, we concluded that these genes do not directly regulate the transcriptional processes of osteoblast differentiation *in vitro*. The decrease in *DEAF1* expression following *TNAP* siRNA treatment, though not statistically significant, suggests that *DEAF1* may function downstream of *TNAP*.

There was a pronounced and statistically significant reduction in metabolic activity in hFOB cells treated with *ACP2* siRNA. This result carried through to the ALP assay, in which staining intensity and ALP+ area fraction were dramatically reduced in only the *TNAP* siRNA and *ACP2* siRNA groups. The combination of these results with the gene expression data suggests that *ACP2* regulates early osteoblast proliferation/viability, but does not directly regulate osteoblast differentiation.

We provide evidence that our approach can steer researchers from GWAS signals toward genes relevant to the pathogenesis of the given trait. Furthermore, because our method treats all genes in implicated TADs equally, functional classification extends to the identification of single variant pleiotropic events; as was the case with an intronic *FTO* variant impacting both *IRX3* and *IRX5* [8].

Despite the advantages presented by TAD_Pathways, the method has a number of limitations. Currently, our method will not overcome the possibility of a gene being inappropriately included in a pathway that it does not actually contribute to, plus all other propagated errors related to pathway curation and analyses [46]. Network based methods built on gene-gene interaction data also suffer from similar biases [47], but potentially to a lesser extent than curated pathways. We include both curated and computationally predicted GO annotations to ameliorate this bias. The computational predictions provide additional support that these genes may be important disease associated genes that we would have missed using only experimentally

validated pathway genes. We are also unable to implicate a gene to a trait if it is not assigned to a curated or predicted pathway, or if it does not fall within a TAD corresponding to a GWAS signal. It is also likely that our approach will not work well with every GWAS. Indeed we are implicating causality to given genes - we are not making a direct connection between the gene and the given variant. Furthermore, our method does not include the possibility of finding genes associated with a disease that is impacted by alternative looping, which has been observed to occur in cancer [48,49] and sickle cell anemia [50]. As research on 3D genome organization increases, it is likely that more diseases will include chromosome looping deficiencies as part of their etiology. Additionally, we used TAD boundaries defined by Dixon *et al.* 2012. A more recent Hi-C analysis at increased resolution substantially reduced the estimated average size of TADs [51]. Nevertheless, there remains disagreement about how TADs are defined [52]. Despite our method using larger TAD boundaries, thus promoting the inclusion of more presumably false positive genes, we retain the ability to identify biologically logical pathways. The larger boundaries permit us to screen a larger number of candidate genes but makes the method analytically conservative by increasing the pathway overrepresentation signal required to surpass the adjusted significance threshold.

The validation screen is also limited: it was performed in a simplified *in vitro* cell culture system lacking organismal complexity, and the cell line selected is largely tetraploid which may partially compensate for gene knockdown. This is particularly true for the lack of reduction in *TNAP* gene expression in the *TNAP* siRNA group, in light of the historical selection of the hFOB cell line based on robust ALP staining in culture [53]. As well, while the TAD approach identifies potentially several GWAS associated genes, herein we only examined two genes per TAD – one immediately adjacent to the GWAS SNP and another that we postulated could play a

role in the skeleton. Further work would need to systematically examine the relative importance of each gene in a TAD.

Other recent mechanisms and algorithms used to assign causality from association signals or enhancers to genes typically leverage multiple data types including expression [54] or epigenetic features [24]. For example, TargetFinder uses several high throughput genomic marks to identify features predictive of a chromosome physically looping together enhancers and promoters [24]. Looping occurs at sub-TAD level resolutions [55] and sub-TADs are variable across cell types. Therefore, in order for a chromosome looping signature to generalize to GWAS signals, a user must assay tissue-specific and high resolution Hi-C to identify more specific interactions. Alternatively, one could also query variants that affect gene expression in high-throughput and systematically match signals to gene expression [56]. A major limitation to these approaches is that several diseases do not yet have a known tissue source or involve multiple tissues. This is particularly true for osteoporosis whereby multiple cell types, as well as systemic factors, influence bone mass [57]. Therefore, identifying these specific signals may require the procedures to be repeated across competing tissue types. In contrast, a TAD_Pathways analysis is computationally cheap and uses publicly available TAD boundaries and GO terms as a guide for assigning genes to GWAS signals. The method is effective in a wide variety of settings and across tissues because TADs are consistent across cell types [25]. In summary, TAD_Pathways can be used to guide researchers toward the most likely causal gene implicated by a GWAS signal. We have also identified *ACP2* as a gene involved in BMD determination, which warrants further investigation.

Conclusions:

TADs offer a novel tool in the investigation of genome function. We present an approach, called TAD_Pathways, to leverage 3D genomics to prioritize and predict causal genes implicated by GWAS signal. At the foundation of our method is the principle that genomic regions within the same TAD more often interact with each other, and therefore, provide the genomic scaffolding that can impact gene function and gene regulation within each TAD. We applied our method to established BMD GWAS signals. By selecting two GWAS signals and two classes of genes for each signal (nearest gene and predicted gene by TAD_Pathways), we demonstrated that our approach can causally implicate genes kilobases away from their associated GWAS signal. We validated *ACP2* (TAD prediction), but not *ARHGAP1* (nearest gene), and show that *ACP2* influences the proliferation and differentiation of osteoblast cells. We were unable to validate either *DEAF1* or *BET1L* and conclude that neither impacts osteoblast gene expression nor metabolic activity. Whether these genes influence other aspects of skeletal biology cannot be determined within the scope of the current study. Future studies focused on BMD GWAS would explore both osteoblast and osteoclast associated changes. In conclusion, as more information and data is collected regarding 3D genome principles, we propose that algorithms that leverage dynamic 3D structure rather than static linear organization will more accurately predict and discover the basic genomic biology of diseases.

Methods:

Data Integration

We used previously identified TAD boundaries for hESC, IMR90, mESC, and mcortex cells for all TAD based analyses [22,58]. To describe the genomic content of TADs, we extracted common SNPs (major allele frequency ≤ 0.95) from the 1000 Genomes Phase III data (2 May

2013 release) [59] and downloaded hg19 Gencode genes [60] and hg19 RepeatMasker repeat elements [61]. We downloaded hg19 FASTA files for all chromosomes as provided by the Genome Reference Consortium [62]. Furthermore, we downloaded the NHGRI-EBI GWAS catalog on 25 February 2016, which holds the significant findings of several GWAS' for over 300 traits [1]. Since the GWAS catalog reports hg38 coordinates, we used the hg38 to hg19 UCSC chain file [63] and PyLiftover [64] to convert genome build coordinates to hg19. We assessed relevant expression quantitative trait loci (eQTLs) using all tissues in the NCBI GTEx eQTL Browser [65].

TAD_Pathways

Our TAD_Pathways method is a light-weight approach that uses TAD boundary regions, rather than distance explicitly, to identify putative causal genes. We first build a comprehensive TAD based gene list that consists of all genes that fall inside TADs that are implicated with a GWAS signal (see **Figure 2**). This gene list assumes that all genes within each signal TAD have an equal likelihood of functional impact on the trait or disease of interest. We then input the TAD based gene list into a WebGestalt overrepresentation analysis [66]. WebGestalt is a webapp that facilitates a pathway analysis interface allowing for quick and custom gene set based analyses. We perform a pathway overrepresentation test for the input TAD based genes against GO biological process, molecular function, and cellular component terms with a background of the human genome. Specifically, this tests if the input gene set is associated with any particular GO term at a higher probability than by chance compared to background genes. We include both experimentally validated and computationally inferred genes in each GO term, which allows the method to discover associations for genes that lack literature support. We

382 consider genes that are annotated to the most significantly enriched GO term to be the associated
383 set [65].
384
385 *Cell culture and siRNA transfection*
386 A human fetal osteoblast cell line (ATCC hFOB 1.19 CRL-11372) was obtained and
387 subcultured twice at 34°C, 5% CO_2 and 95% relative humidity in 1:1 DMEM/F12 with 2.5mM
388 L-glutamine without phenol red (Gibco 21041025) supplemented with 10% FBS (Atlas USDA
389 F0500D) and 0.3mg/mL G418 sulfate (Gibco 10131035). All experiments were conducted in
390 three temporally separated independent technical replicates from cryopreserved P2 aliquots of
391 these cells. 48 hours prior to transfection, media was switched to a G418-free formulation.
392 Transfections were conducted in single-cell suspension using a commercial siRNA reagent
393 system (Santa Cruz sc-45064) according to the manufacturer's instructions, with 6µL of siRNA
394 duplex and 4µL transfection reagent in 750µL of transfection media per 100,000 cells. Following
395 trypsinization, cells were counted and divided into one of 8 experimental groups: 1) untreated
396 control, 2) siRNA-negative transfection reagent control, 3) scrambled control siRNA (sc-37007),
397 4) *TNAP* siRNA (sc-38921), 5) *ARHGAP1* siRNA (sc-96477), 6) *ACP2* siRNA (sc-96327), 7)
398 *BET1L* siRNA (sc-97007) or 8) Suppressin (*DEAF1*) siRNA (sc-76613). Samples for RNA
399 isolation were generated by plating 200,000 cells per well in tissue culture treated 6-well plates
400 (Falcon 353046). Samples for MTT assay and alkaline phosphatase (ALP) staining were
401 generated by plating 50,000 cells per well in tissue culture treated 24-well plates (Falcon
402 353047). Cells were then switched to a 37°C incubator and transfected for 6 hours, at which
403 point transfection cocktails were diluted with 2x hFOB media concentrate. Media was
404 completely changed to 1x standard hFOB media 16 hours later.

405

406 *Quantitative PCR*

407 RNA was harvested at Day 4 using TRIzol (Ambion) followed by acid guanidinium
408 thiocyanate-phenol-chloroform extraction and RNeasy (Qiagen) spin-column purification with
409 DNase (Qiagen) then reverse-transcribed using a high-capacity RNA-to-cDNA kit (Applied
410 Biosystems). Duplicate qPCR reactions were conducted on 20ng of whole-RNA template using
411 SYBR Select master mix (Applied Biosystems) in an Applied Biosystems 7500 Fast Real-Time
412 PCR System. Primers for *GAPDH*, *OSX*, *OCN* and *IBSP* were adopted from the literature and
413 synthesized by R&D Systems. New primer sets spanning exon-exon junctions were designed for
414 *ARHGAP1*, *ACP2*, *BET1L* and *DEAF1* using NCBI Primer Blast, verified by melt curve analysis
415 and agarose gel electrophoresis. Sequences follow: *ARHGAP1* F-
416 GCGGAAATGGTTGGGGATAG R-CCTTAAGAGAAACCGCGCTC (127bp), *ACP2* F-
417 AGCGGGTTCCAGCTTGTTT R-TGGCGGTACAGCAAGGTAAC (165bp), *BET1L* F-
418 GGATGGCATGGACTCGGATT R-TCCTCTGGAGCCCAAAACAC (254bp), *DEAF1* F-
419 GGAAGGAGCAGTCCTGCGTT R-TCACCTTCTCCATCACGCTTT (195bp). Results were
420 analyzed using the 2^{-ddCt} method using GAPDH as a housekeeping gene and reported as (mean ±
421 standard deviation) fold-change versus untreated controls. Statistical significance was
422 determined using 2-way homoscedastic Student's t-tests versus the scrambled siRNA control,
423 annotated using *$p \leq 0.05$ and #$p \leq 0.10$. The acronym N.S. stands for "not significant".

424

425 *MTT metabolic assay*

426 Cellular metabolism/proliferation was assessed using a commercial cell growth
427 determination kit (Sigma CGD1). At 1 or 4 days post-transfection, media in assigned 24-well

plates was switched to 450µL hFOB media plus 50µL MTT solution. Cells were incubated at 37°C for 3.5 hours, after which the media was aspirated and the resulting formazan crystals were solubilized in MTT solvent. Plates were shaken and read in a BioTek Synergy H1 microplate reader. Results are reported as the difference in mean absorbance at 570nm-690nm from Day 1 to Day 4. Error bars represent root-mean-square standard deviation from the measurements at both days. Statistical significance was determined using 2-way homoscedastic Student's t-tests versus the scrambled siRNA control, annotated using *$p \leq 0.05$ and #$p \leq 0.10$.

Alkaline phosphatase (ALP) staining

Plates were stained at 4 days post-transfection using a commercial ALP kit (Sigma 86C). Dried plates were then imaged at 600dpi using an Epson V370 photo scanner and staining was quantified using mean whole-well intensity measurements in ImageJ using raw output files. ALP area fraction was calculated using color thresholding. Values are reported as mean ± standard deviation. Statistical significance was determined using 2-way homoscedastic Student's t-tests versus the scrambled siRNA control, annotated using *$p \leq 0.05$ and #$p \leq 0.10$. Images of plates presented as figures were edited using a warming filter and for brightness/contrast using Adobe Photoshop CS6.

Computational Reproducibility

We provide all of our source code under a permissive open source license and encourage others to modify and build upon our work [67]. Additionally, we provide an accompanying docker image [68] to replicate our computational environment (https://hub.docker.com/r/gregway/tad_pathways/) [69].

Declarations:

Ethics approval and consent to participate

Not applicable.

Consent for publication

Not applicable.

Availability of data and material

All data used to construct the TAD_Pathways approach are publically available datasets. We make all software used to develop this approach publically available in a GitHub repository (http://github.com/greenelab/tad_pathways). We also provide a docker image (https://hub.docker.com/r/gregway/tad_pathways/) and archive the GitHub software on Zenodo (https://zenodo.org/record/163950).

Competing interests

The authors declare no competing interests.

Funding

This work was supported by the Genomics and Computational Biology Graduate program at The University of Pennsylvania (to G.P.W.); the Gordon and Betty Moore Foundation's Data Driven Discovery Initiative (grant number GBMF 4552 to C.S.G); the National Institute of Dental & Craniofacial Research (grant number NIH F32DE026346 to D.W.Y.); S.F.A.G is supported by the Daniel B. Burke Endowed Chair for Diabetes Research.

Authors' contributions

GPW wrote the software, analyzed the data, developed the method and wrote the manuscript; DWY performed the experimental validation and wrote the manuscript; KDH performed the

474 experimental validation and wrote the manuscript; CSG analyzed the data, developed the
475 method and wrote the manuscript; SFAG analyzed the data, developed the method and wrote
476 the manuscript.

477 *Acknowledgements*

478 Hannah E. Sexton and Troy L. Mitchell assisted in optimizing siRNA transfection
479 conditions. Daniel Himmelstein and Amy Campbell performed analytical code review.

480 *Authors' information (optional)*

481

482

483

484

485

486

487

488

489

490

491

492

493

494

495

496

Supplementary Figures:

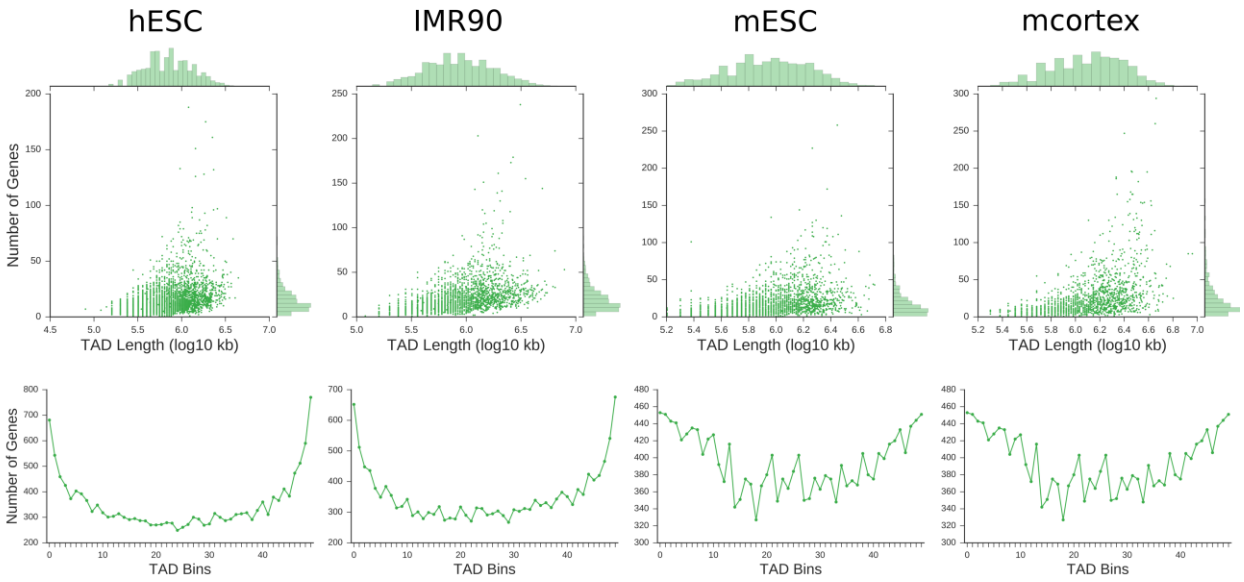

Supplementary Figure S1: *Distributions of genes across topologically associating domains of four cell types.* Bars on the top and right side of the plots represent histograms of each respective metric. We independently discretized TADs into 50 bins where the distribution of elements is linear from 5' to 3' (bin 0 is the 5' most end of all TADs).

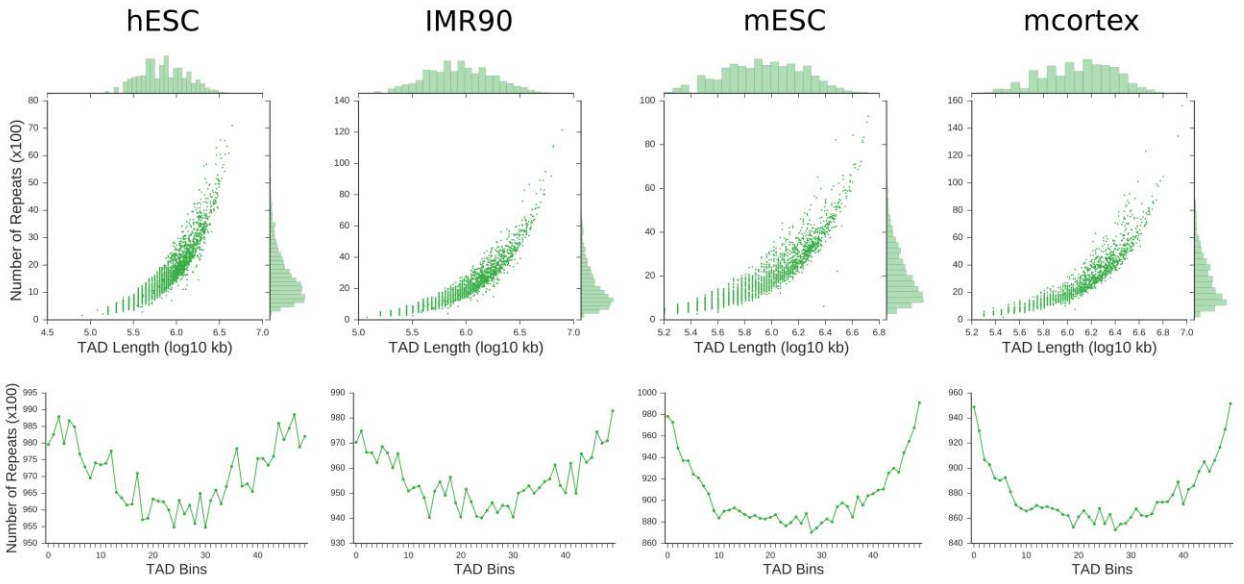

Supplementary Figure S2: *Distributions of all repeat elements across topologically associating domains of four cell types.* Bars on the top and right side of the plots represent histograms of each respective metric. We independently discretized TADs into 50 bins where the distribution of elements is linear from 5' to 3' (bin 0 is the 5' most end of all TADs).

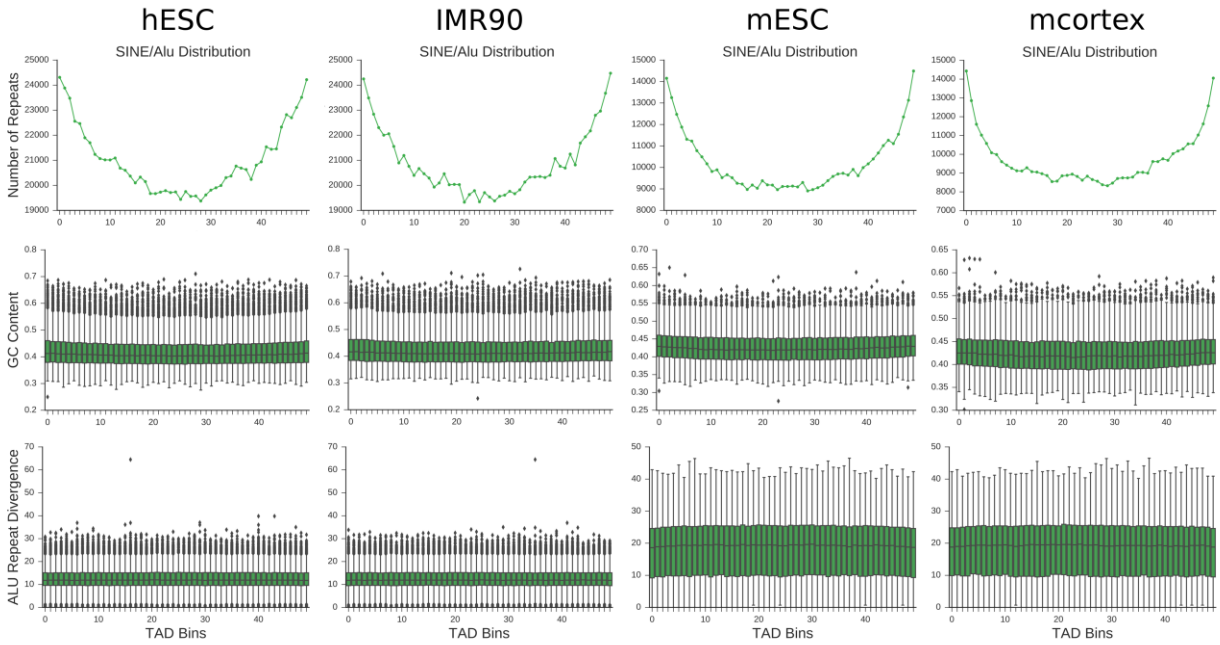

Supplementary Figure S3: *Distributions of SINE/Alu elements and potential confounding factors across topologically associating domains of four cell types.* We independently discretized TADs into 50 bins where the distribution of elements is linear from 5' to 3' (bin 0 is the 5' most end of all TADs). The distribution of Alu elements is strongly clustered toward TAD boundaries but neither the percentage of GC content across TADs nor the evolutionary divergence of Alu elements can explain the Alu distribution.

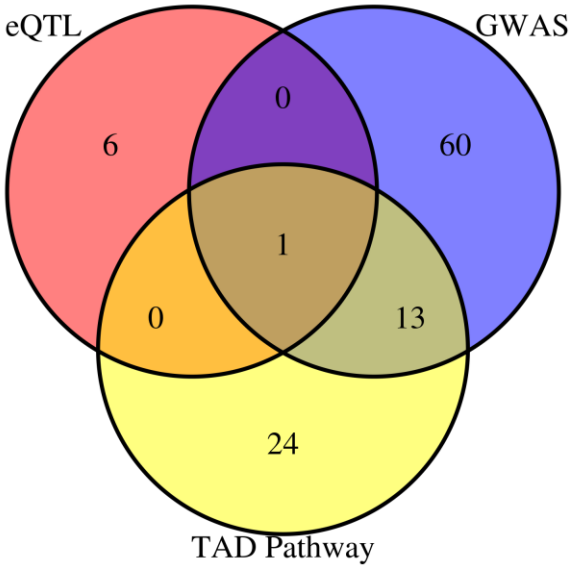

Supplementary Figure S4: *Bone Mineral Density gene counts associated with various classes of evidence.* The gene *LRP5* is implicated by all evidence codes. About 1/3 of all TAD_Pathways implicated genes are the nearest gene implicated by the GWAS signal.

Tables:

Supplementary Table S1: *Chi square testing the enrichment of genes at TAD boundaries and enrichment of SNPs towards the right half of TADs.*

	Enrichment of SNPs in the Right of TADs			
	Left	Right	Chi-square	P
hESC	3268781	3296450	116.6	3.5E-27
IMR90	3211140	3210251	0.12	0.73
mESC*	25161934	25129279	21.2	4.1E-06
mcortex	24616532	24641931	13.1	3.0E-4

* Note- mouse embryonic stem cells have an opposite enrichment. There are more SNPs in the left of TADs

We provide **Supplementary Tables S2** and **S3** as attached .xls files.

Abbreviations:

TAD – Topologically associating domain

GWAS – Genome wide association study

SNP – Single nucleotide polymorphism

BMD – Bone mineral density

hESC – Human embryonic stem cells

mESC – Mouse embryonic stem cells

IMR90 – Human fibroblast cells

mcortex – Mouse cortex cells

siRNA – Small interfering RNA

eQTL – Expression quantitative trail loci

hFOB – Human fetal osteoblast

543 TNAP - tissue-nonspecific alkaline phosphatase

544 OCN – osteocalcin

545 IBSP – bone sialoprotein

546 ALP – Alkaline phosphatase

547 GO – Gene ontology

548 eQTL – Expression quantitative trait loci

549

550 **References:**

551 1. Welter D, MacArthur J, Morales J, Burdett T, Hall P, Junkins H, et al. The NHGRI GWAS
552 Catalog, a curated resource of SNP-trait associations. Nucleic Acids Res. 2014;42:D1001–6.

553 2. Zhang F, Lupski JR. Non-coding genetic variants in human disease. Hum. Mol. Genet.
554 2015;24:R102–10.

555 3. Ward LD, Kellis M. Interpreting noncoding genetic variation in complex traits and human
556 disease. Nat. Biotechnol. 2012;30:1095–106.

557 4. McVean GA, Altshuler (Co-Chair) DM, Durbin (Co-Chair) RM, Abecasis GR, Bentley DR,
558 Chakravarti A, et al. An integrated map of genetic variation from 1,092 human genomes. Nature.
559 2012;491:56–65.

560 5. Brodie A, Azaria JR, Ofran Y. How far from the SNP may the causative genes be? Nucleic
561 Acids Res. 2016;gkw500.

562 6. Tung YCL, Yeo GSH, O'Rahilly S, Coll AP. Obesity and FTO: Changing Focus at a Complex
563 Locus. Cell Metab. 2014;20:710–8.

564 7. Ragvin A, Moro E, Fredman D, Navratilova P, Drivenes O, Engstrom PG, et al. Long-range
565 gene regulation links genomic type 2 diabetes and obesity risk regions to HHEX, SOX4, and
566 IRX3. Proc. Natl. Acad. Sci. 2010;107:775–80.

567 8. Claussnitzer M, Dankel SN, Kim K-H, Quon G, Meuleman W, Haugen C, et al. *FTO* Obesity
568 Variant Circuitry and Adipocyte Browning in Humans. N. Engl. J. Med. 2015;373:895–907.

569 9. Smemo S, Tena JJ, Kim K-H, Gamazon ER, Sakabe NJ, Gómez-Marín C, et al. Obesity-
570 associated variants within FTO form long-range functional connections with IRX3. Nature.
571 2014;507:371–5.

572 10. Grant SFA, Thorleifsson G, Reynisdottir I, Benediktsson R, Manolescu A, Sainz J, et al.
573 Variant of transcription factor 7-like 2 (TCF7L2) gene confers risk of type 2 diabetes. Nat.
574 Genet. 2006;38:320–3.

575 11. Xia Q, Chesi A, Manduchi E, Johnston BT, Lu S, Leonard ME, et al. The type 2 diabetes
576 presumed causal variant within TCF7L2 resides in an element that controls the expression of
577 ACSL5. Diabetologia. 2016;59:2360–8.

578 12. Herman MA, Rosen ED. Making Biological Sense of GWAS Data: Lessons from the FTO
579 Locus. Cell Metab. 2015;22:538–9.

580 13. Dekker J, Rippe K, Dekker M, Kleckner N. Capturing chromosome conformation. Science.
581 2002;295:1306–11.

582 14. Dekker J. Gene Regulation in the Third Dimension. Science. 2008;319:1793–4.

583 15. Lieberman-Aiden E, van Berkum NL, Williams L, Imakaev M, Ragoczy T, Telling A, et al.
584 Comprehensive Mapping of Long-Range Interactions Reveals Folding Principles of the Human
585 Genome. Science. 2009;326:289–93.

586 16. Duan Z, Andronescu M, Schutz K, McIlwain S, Kim YJ, Lee C, et al. A three-dimensional
587 model of the yeast genome. Nature. 2010;465:363–7.

588 17. Phillips-Cremins JE, Sauria MEG, Sanyal A, Gerasimova TI, Lajoie BR, Bell JSK, et al.
589 Architectural Protein Subclasses Shape 3D Organization of Genomes during Lineage
590 Commitment. Cell. 2013;153:1281–95.

591 18. Sexton T, Yaffe E, Kenigsberg E, Bantignies F, Leblanc B, Hoichman M, et al. Three-
592 Dimensional Folding and Functional Organization Principles of the Drosophila Genome. Cell.
593 2012;148:458–72.

594 19. Symmons O, Uslu VV, Tsujimura T, Ruf S, Nassari S, Schwarzer W, et al. Functional and
595 topological characteristics of mammalian regulatory domains. Genome Res. 2014;24:390–400.

596 20. Pope BD, Ryba T, Dileep V, Yue F, Wu W, Denas O, et al. Topologically associating
597 domains are stable units of replication-timing regulation. Nature. 2014;515:402–5.

598 21. Gurudatta B, Yang J, Van Bortle K, Donlin-Asp P, Corces V. Dynamic changes in the
599 genomic localization of DNA replication-related element binding factor during the cell cycle.
600 Cell Cycle. 2013;12:1605–15.

601 22. Dixon JR, Selvaraj S, Yue F, Kim A, Li Y, Shen Y, et al. Topological domains in
602 mammalian genomes identified by analysis of chromatin interactions. Nature. 2012;485:376–80.

603 23. Nora EP, Dekker J, Heard E. Segmental folding of chromosomes: A basis for structural and
604 regulatory chromosomal neighborhoods?: Prospects & Overviews. BioEssays.
605 2013;35:818–28.

606 24. Whalen S, Truty RM, Pollard KS. Enhancer–promoter interactions are encoded by complex
607 genomic signatures on looping chromatin. Nat. Genet. 2016;48:488–96.

608 25. Smith EM, Lajoie BR, Jain G, Dekker J. Invariant TAD Boundaries Constrain Cell-Type-
609 Specific Looping Interactions between Promoters and Distal Elements around the CFTR Locus.
610 Am. J. Hum. Genet. 2016;98:185–201.

611 26. Richards JB, Rivadeneira F, Inouye M, Pastinen TM, Soranzo N, Wilson SG, et al. Bone
612 mineral density, osteoporosis, and osteoporotic fractures: a genome-wide association study.
613 Lancet Lond. Engl. 2008;371:1505–12.

614 27. Rivadeneira F, Styrkársdottir U, Estrada K, Halldórsson BV, Hsu Y-H, Richards JB, et al.
615 Twenty bone-mineral-density loci identified by large-scale meta-analysis of genome-wide
616 association studies. Nat. Genet. 2009;41:1199–206.

617 28. Estrada K, Styrkarsdottir U, Evangelou E, Hsu Y-H, Duncan EL, Ntzani EE, et al. Genome-
618 wide meta-analysis identifies 56 bone mineral density loci and reveals 14 loci associated with
619 risk of fracture. Nat. Genet. 2012;44:491–501.

620 29. Styrkarsdottir U, Thorleifsson G, Sulem P, Gudbjartsson DF, Sigurdsson A, Jonasdottir A, et
621 al. Nonsense mutation in the LGR4 gene is associated with several human diseases and other
622 traits. Nature. 2013;497:517–20.

623 30. Hendrickx G, Boudin E, Van Hul W. A look behind the scenes: the risk and pathogenesis of
624 primary osteoporosis. Nat. Rev. Rheumatol. 2015;11:462–74.

625 31. Choo SY. The HLA System: Genetics, Immunology, Clinical Testing, and Clinical
626 Implications. Yonsei Med. J. 2007;48:11.

627 32. Håvik B, Le Hellard S, Rietschel M, Lybæk H, Djurovic S, Mattheisen M, et al. The
628 Complement Control-Related Genes CSMD1 and CSMD2 Associate to Schizophrenia. Biol.
629 Psychiatry. 2011;70:35–42.

630 33. Kwon E, Wang W, Tsai L-H. Validation of schizophrenia-associated genes CSMD1,
631 C10orf26, CACNA1C and TCF4 as miR-137 targets. Mol. Psychiatry. 2013;18:11–2.

632 34. Wang K, Li M, Bucan M. Pathway-Based Approaches for Analysis of Genomewide
633 Association Studies. Am. J. Hum. Genet. 2007;81:1278–83.

634 35. Hao K, Di X, Cawley S. LdCompare: rapid computation of single- and multiple-marker r2
635 and genetic coverage. Bioinformatics. 2007;23:252–4.

636 36. Taşan M, Musso G, Hao T, Vidal M, MacRae CA, Roth FP. Selecting causal genes from
637 genome-wide association studies via functionally coherent subnetworks. Nat. Methods.
638 2014;12:154–9.

639 37. Ashburner M, Ball CA, Blake JA, Botstein D, Butler H, Cherry JM, et al. Gene Ontology:
640 tool for the unification of biology. Nat. Genet. 2000;25:25–9.

641 38. Petersen A, Alvarez C, DeClaire S, Tintle NL. Assessing Methods for Assigning SNPs to
642 Genes in Gene-Based Tests of Association Using Common Variants. Chen L, editor. PLoS ONE.
643 2013;8:e62161.

644 39. Mu XJ, Lu ZJ, Kong Y, Lam HYK, Gerstein MB. Analysis of genomic variation in non-
645 coding elements using population-scale sequencing data from the 1000 Genomes Project.
646 Nucleic Acids Res. 2011;39:7058–76.

647 40. Jurka J, Kohany O, Pavlicek A, Kapitonov VV, Jurka MV. Duplication, coclustering, and
648 selection of human Alu retrotransposons. Proc. Natl. Acad. Sci. 2004;101:1268–72.

649 41. Deininger P. Alu elements: know the SINEs. Genome Biol. 2011;12:236.

650 42. Wang J, Vicente-García C, Seruggia D, Moltó E, Fernandez-Miñán A, Neto A, et al. MIR
651 retrotransposon sequences provide insulators to the human genome. Proc. Natl. Acad. Sci.
652 2015;112:E4428–37.

653 43. Gu Z, Jin K, Crabbe MJC, Zhang Y, Liu X, Huang Y, et al. Enrichment analysis of Alu
654 elements with different spatial chromatin proximity in the human genome. Protein Cell.
655 2016;7:250–66.

656 44. Baron R, Kneissel M. WNT signaling in bone homeostasis and disease: from human
657 mutations to treatments. Nat. Med. 2013;19:179–92.

658 45. Krishnan V, Bryant HU, Macdougald OA. Regulation of bone mass by Wnt signaling. J.
659 Clin. Invest. 2006;116:1202–9.

660 46. Khatri P, Sirota M, Butte AJ. Ten Years of Pathway Analysis: Current Approaches and
661 Outstanding Challenges. Ouzounis CA, editor. PLoS Comput. Biol. 2012;8:e1002375.

662 47. Reguly T, Breitkreutz A, Boucher L, Breitkreutz B-J, Hon GC, Myers CL, et al.
663 Comprehensive curation and analysis of global interaction networks in Saccharomyces
664 cerevisiae. J. Biol. 2006;5:11.

665 48. Corces MR, Corces VG. The three-dimensional cancer genome. Curr. Opin. Genet. Dev.
666 2016;36:1–7.

667 49. Flavahan WA, Drier Y, Liau BB, Gillespie SM, Venteicher AS, Stemmer-Rachamimov AO,
668 et al. Insulator dysfunction and oncogene activation in IDH mutant gliomas. Nature.
669 2015;529:110–4.

670 50. Deng W, Lee J, Wang H, Miller J, Reik A, Gregory PD, et al. Controlling long-range
671 genomic interactions at a native locus by targeted tethering of a looping factor. Cell.
672 2012;149:1233–44.

673 51. Rao SSP, Huntley MH, Durand NC, Stamenova EK, Bochkov ID, Robinson JT, et al. A 3D
674 Map of the Human Genome at Kilobase Resolution Reveals Principles of Chromatin Looping.
675 Cell. 2014;159:1665–80.

676 52. Bonev B, Cavalli G. Organization and function of the 3D genome. Nat. Rev. Genet.
677 2016;17:661–78.

678 53. Harris SA, Enger RJ, Riggs BL, Spelsberg TC. Development and characterization of a
679 conditionally immortalized human fetal osteoblastic cell line. J. Bone Miner. Res. Off. J. Am.
680 Soc. Bone Miner. Res. 1995;10:178–86.

681 54. Zhu Z, Zhang F, Hu H, Bakshi A, Robinson MR, Powell JE, et al. Integration of summary
682 data from GWAS and eQTL studies predicts complex trait gene targets. Nat. Genet.
683 2016;48:481–7.

684 55. Dowen JM, Fan ZP, Hnisz D, Ren G, Abraham BJ, Zhang LN, et al. Control of Cell Identity
685 Genes Occurs in Insulated Neighborhoods in Mammalian Chromosomes. Cell. 2014;159:374–
686 87.

687 56. Tewhey R, Kotliar D, Park DS, Liu B, Winnicki S, Reilly SK, et al. Direct Identification of
688 Hundreds of Expression-Modulating Variants using a Multiplexed Reporter Assay. Cell.
689 2016;165:1519–29.

690 57. Lupsa BC, Insogna K. Bone Health and Osteoporosis. Endocrinol. Metab. Clin. North Am.
691 2015;44:517–30.

692 58. Ho JWK, Jung YL, Liu T, Alver BH, Lee S, Ikegami K, et al. Comparative analysis of
693 metazoan chromatin organization. Nature. 2014;512:449–52.

694 59. 1000 Genomes Project Consortium, Auton A, Brooks LD, Durbin RM, Garrison EP, Kang
695 HM, et al. A global reference for human genetic variation. Nature. 2015;526:68–74.

696 60. Harrow J, Frankish A, Gonzalez JM, Tapanari E, Diekhans M, Kokocinski F, et al.
697 GENCODE: The reference human genome annotation for The ENCODE Project. Genome Res.
698 2012;22:1760–74.

699 61. Smit A, Hubley R, Green P. RepeatMasker Open-4.0 [Internet]. Available from:
700 http://www.repeatmasker.org

701 62. Church DM, Schneider VA, Graves T, Auger K, Cunningham F, Bouk N, et al. Modernizing
702 Reference Genome Assemblies. PLoS Biol. 2011;9:e1001091.

703 63. Kent WJ, Sugnet CW, Furey TS, Roskin KM, Pringle TH, Zahler AM, et al. The Human
704 Genome Browser at UCSC. Genome Res. 2002;12:996–1006.

705 64. Tretyakov K. pyliftover [Internet]. 2014. Available from:
706 https://github.com/konstantint/pyliftover

707 65. GTEx Consortium. The Genotype-Tissue Expression (GTEx) project. Nat. Genet.
708 2013;45:580–5.

709 66. Wang J, Duncan D, Shi Z, Zhang B. WEB-based GEne SeT AnaLysis Toolkit (WebGestalt):
710 update 2013. Nucleic Acids Res. 2013;41:W77–83.

711 67. Gregory Way, Casey Green. Greenelab/Tad_Pathways: Pre-Release. 2016 [cited 2016 Nov
712 14]; Available from: https://doi.org/10.5281/zenodo.163950

713 68. Boettiger C. An introduction to Docker for reproducible research. ACM SIGOPS Oper. Syst.
714 Rev. 2015;49:71–9.

715 69. Gregory Way, Struan Grant, Casey Greene. TAD Pathways Archived Docker Image. 2016
716 [cited 2016 Nov 14]; Available from: https://doi.org/10.5281/zenodo.166556

717